POLITECNICO DI TORINO
Repository ISTITUZIONALE

On the Development of Sustainable Covalent Adaptable Networks Based on Epoxidized Soybean Oil Acrylate and Cystamine

Original
On the Development of Sustainable Covalent Adaptable Networks Based on Epoxidized Soybean Oil Acrylate and Cystamine / Giribaldi, L., Damonte, G., Fina, A., Noe, C., Pellis, A., Monticelli, O.. - In: JOURNAL OF POLYMERS AND THE ENVIRONMENT. - ISSN 1566-2543. - STAMPA. - 34:8(2026), pp. 1-19. [10.1007/s10924-026-03915-2]

Availability:
This version is available at: 11583/3017229 since: 2026-10-30T09:31:20Z

Publisher:
Springer

Published
DOI:10.1007/s10924-026-03915-2

Terms of use:

This article is made available under terms and conditions as specified in the corresponding bibliographic description in the repository

Publisher copyright

(Article begins on next page)

17 November 2026

Journal of Polymers and the Environment (2026) 34:197
https://doi.org/10.1007/s10924-026-03915-2

ORIGINAL PAPER

On the Development of Sustainable Covalent Adaptable Networks Based on Epoxidized Soybean Oil Acrylate and Cystamine

Leonardo Giribaldi[1] · Giacomo Damonte[1] · Alberto Fina[2] · Camilla Noè[3] · Alessandro Pellis[1] · Orietta Monticelli[1]

Received: 31 March 2026 / Accepted: 6 July 2026 / Published online: 14 July 2026
© The Author(s) 2026

Abstract

The work focuses on the design of sustainable materials that meet key environmental requirements, including the bio-based origin of starting compounds, environmentally friendly preparation methods, as well as easy recyclability and biodegradation at the end of life. To this end, systems based on reagents from renewable sources, such as epoxidized soybean oil acrylate (ESOA) and cystamine (Cys) as a crosslinker, were developed to form covalent adaptable networks (CANs), using a simple reaction carried out under mild conditions, without the need for solvent or catalyst. Two different molar ratios between the acrylate groups of ESOA and the amino groups of Cys were investigated (1:1, ESOA-Cys_1:1 and 2:1, ESOA-Cys_2:1). The Aza–Michael reaction between the two components was confirmed and monitored during curing at different temperatures by IR spectroscopy, revealing distinct kinetic behaviors for the two formulations, a phenomenon attributed to a change in the reaction mechanism. In both cases, network formation was confirmed by gel fraction (GF%) analysis, which reached 100%, indicating complete cross-linking after 6 h under all temperature conditions tested. DSC measurements of the two formulations were recorded over time, curing the samples at 100 °C, the temperature characterized by the fastest kinetics among those investigated. The glass transition temperature (T_g) of the formulations was found to gradually increase over time during curing, with the formulations reaching comparable T_g values of -3 °C and −4 °C for 1:1 and 2:1, respectively, which levelled off to the same value of -2 °C after 2 days, thus demonstrating the formation of crosslinks within the systems and confirming the effectiveness of the curing time used for sample preparation. DMTA and rheological measurements of the cured samples revealed the formation of more rigid networks in ESOA-Cys_2:1, attributed to a higher crosslinking density, while stress-relaxation experiments demonstrated the dynamic nature of the networks in both formulations, although the relaxation behavior depended on the acrylate: amino groups molar ratio, reflecting the crosslinking density. Finally, the developed CANs exhibited excellent recyclability and self-healing properties when heated to 180 °C and were completely degraded by enzymatic hydrolysis.

Introduction

Covalent adaptable networks (CANs), especially those considered bio-based, i.e., made from compounds derived from renewable sources, are of great interest not only for academic research but also for potential industrial applications [1]. Indeed, CANs are a novel class of polymers that combine the properties of thermoplastics and thermosets by incorporating dynamic covalent bonds within a cross-linked architecture, allowing flow through network rearrangements [2]. In addition to improving the specific properties of polymer formulations, CANs meet sustainability requirements, as they can be recycled thanks to the formation of a dynamic network [3, 4]. There are several examples of the development of such "green" materials, where monomers from renewable sources have been considered, characterized by

✉ Alessandro Pellis
alessandro.pellis@unige.it

✉ Orietta Monticelli
orietta.monticelli@unige.it

[1] Dipartimento di Chimica e Chimica Industriale, Università degli Studi di Genova, Via Dodecaneso 31, Genoa 16146, Italy

[2] Dipartimento di Scienza Applicata e Tecnologia, Politecnico di Torino, Viale Teresa Michel 5, Alessandria, Italy

[3] Dipartimento di Scienza Applicata e Tecnologia, Politecnico di Torino, C.so Duca Degli Abruzzi 24, Torino 10129, Italy

chemical properties that make them suitable for the development of non-permanent cross-linked systems [5–8]. Among the renewable feedstocks that can be used for the CANs production, vegetable oils (VOs), obtained from widely available sources such as seeds, prove to be ideal systems for this use due to their low cost, non-toxicity, availability, biodegradability, and chemical structure based on unsaturation, allowing tailored and easy chemical modification [9–14]. In particular, soybean oil, namely the second most produced VO in the world, accounting for approximately 30% of global production volume [15] Recently, this compound has been used in the synthesis of copolymers based on hydrogen bond crosslinked networks [16] and polyurethanes [17] for use as adhesives, as well as in the development of non-isocyanate polyurethane coatings [18] and nanocomposite materials [19]. Moreover, soybean oil is easily functionalized to epoxidized soybean oil acrylate (ESOA). ESOA, the subject of the study, could be effectively used for the development of CANs formulations due to both its cost and chemical properties [12, 20–23]. Indeed, ESOA is a semisynthetic viscous liquid obtained from soybean oil in a two-step process [24]. In the first step, the double bonds of soybean oil are epoxidized using a formic acid/H_2O_2 mixture to form epoxidized soybean oil (ESO). In the second phase, the oxirane rings present in the obtained ESO are reacted with acrylic acid to form acrylic esters and hydroxyl groups [25]. Recently, some studies have highlighted the possibility of obtaining acrylic acid from renewable sources, thereby enabling the production of a 100% bio-based ESOA [26]. Clearly, the presence of acrylic moieties allows the use of ESOA alone or in the preparation of systems with a wide range of crosslinking agents [27]. In the development of CANs, there are many examples related to the use of bio-based materials [28, 29], including ESOA [30, 31]. For example, Zych et al. developed ESOA-based vitrimers, namely CANs based on an associative mechanism, by exploiting a thiol-ene reaction with a dynamic boronic ester chemistry-based crosslinker (DBEDT) under solventless conditions [30]. This system, characterized by a glass transition temperature (T_g) of 2 °C, exhibited high dynamicity due to the bond rearrangement ability enabled by the fast boronic ester metathesis reaction. This property was reflected in a very low activation energy for the relaxation process (29 kJ/mol). In addition, the possibility of self-healing within 24 h at room temperature was validated, and its optimal adhesion to several substrates disclosed its potential application as smart coatings. Furthermore, it was demonstrated that this vitrimer can be chemically recycled by simply dissolving it in 90% EtOH, allowing the recovery of neat material by casting the resulting solution. ESOA was also employed by Cvek et al. in the development of self-healing, recyclable, bio-based magnetic composite vitrimers [31]. In this case, ESOA was modified by adding carbonyl iron (CI) magnetic particles (60, 70, and 80 wt%) before the crosslinking reaction with DBEDT to form a dynamic network acting as a host for the ferromagnetic material. Indeed, when exposed to magnetic fields, the composite systems were found to be characterized by remarkable relative magnetorheological properties, comparable to magnetic composites based on vulcanized matrices, and excellent electromagnetic interference shielding capability within the X-band frequency. As in the previous example, these magnetic composites demonstrated autonomous self-healing as well as the ability for directional healing when exposed to a magnetic field. Moreover, these systems could be reprocessed several times by compression molding or dissolution in 90% EtOH, demonstrating that these materials can be used multiple times without generating waste.

Although these studies highlight the potential of ESOA for the production of high-performance materials, its use in the development of CAN systems undergoes to the same limitations as many other bio-based components, as the entire formulations are usually only partially bio-based, as they consist not only of ESOA, a component from renewable sources, but also of crosslinking agents, which are usually based on fossil raw materials or toxic substances, posing a significant challenge to the sustainability of the material [32]. To overcome these limitations, these compounds need to be replaced with accessible, “green” components to produce 100% renewable systems. Furthermore, to make the entire process fully environmentally friendly, easily scalable preparation methods that do not rely on the use of solvents or catalysts need to be applied. With this in mind, ESOA was combined for the first time in this work with a bio-based crosslinker, namely cystamine (Cys), which is characterized by amino groups and an exchangeable disulfide bridge [33, 34]. Cys is commonly considered a potentially bio-based component, as it can be synthesized by oxidation of cysteamine under mild conditions. Cysteamine is the decarboxylated derivative of L-cysteine, a naturally occurring amino acid and a major constituent of keratin, which can be obtained from renewable resources [35].

Indeed, with this compound, it is potentially possible to achieve crosslinking by an Aza-Michael reaction between the acrylate groups of ESOA and the amino groups of Cys, which behave as Michael acceptors and donors, respectively [36, 37]. This type of reaction meets the principles of click chemistry, being characterized by high reaction rates and conversion, does not require a catalyst, and proceeds under mild conditions (i.e., at room temperature) without the formation of undesired by-products [38, 39]. Since both ESOA and Cys are liquid at room temperature, they can be mixed without the use of solvents, making the process even more attractive from both a chemical and environmental point of

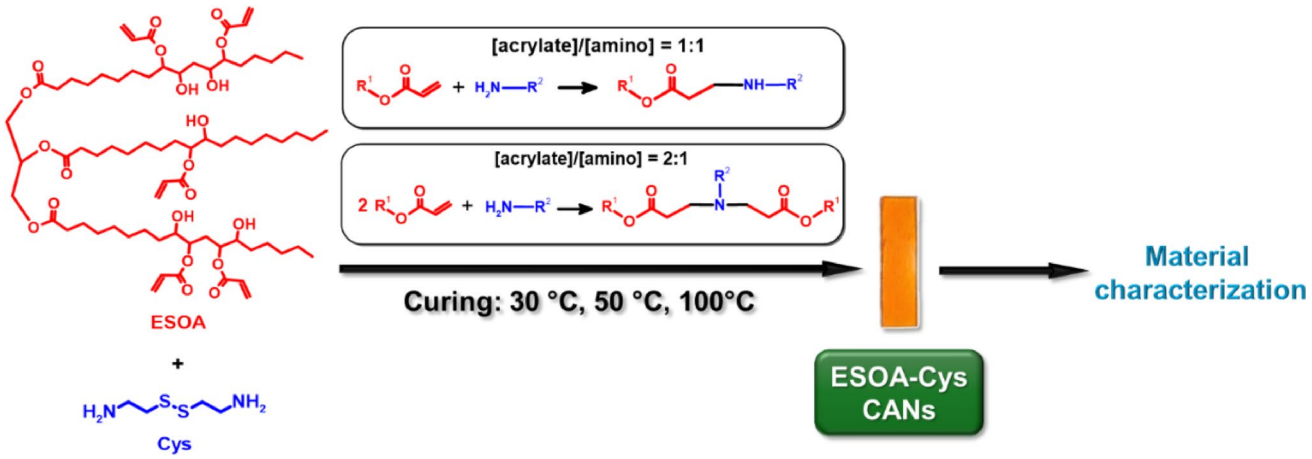


Fig. 1 Scheme of CAN preparation procedure

Table 1 Characteristics of the prepared ESOA-Cys samples

Sample	[acrylate]/[amino]	Volume of Cys added to 1 g of ESOA [µl]	Curing temperature [°C]
ESOA-Cys_1:1_30	1:1	180	30
ESOA-Cys_1:1_50	1:1	180	50
ESOA-Cys_1:1_100	1:1	180	100
ESOA-Cys_2:1_30	2:1	90	30
ESOA-Cys_2:1_50	2:1	90	50
ESOA-Cys_2:1_100	2:1	90	100

view (Fig. 1). Furthermore, in contrast to the previous literature, not only the material properties were evaluated, but also the kinetics of the crosslinking process as a function of the composition of the reaction mixture, as well as the enzymatic hydrolysis of the resulting materials, were investigated in detail by using *Humicola insolens* Cutinase with this kind of system for the first time.

Experimental

Materials

Epoxidized soybean oil acrylate (ESOA), m.w. = 1400 g/mol, 3.4 acrylates/molecule, cystamine dihydrochloride (Cys.2HCl) > 98%, potassium hydroxide (KOH) > 85%, dichloromethane (DCM), and toluene anhydrous > 99% were purchased from Sigma-Aldrich. All reactants, except Cys.2HCl, were used as received without further purification.

Cystamine (Cys) Crosslinker Preparation

The Cystamine (Cys) was purified according to the procedure previously described by Roig et al. [33]. Specifically, 4.00 g of cystamine dichloride was dissolved in 16 mL of Milli-Q water at room temperature under stirring, and then 12 mL of an aqueous 20% m/V KOH solution was added until the pH reached 13, which was adjusted by adding more KOH solution. The resulting solution was then transferred to a separatory funnel and extracted with three 12 mL portions of DCM. The collected organic phases from the extractions were dried over 5.00 g anhydrous $MgSO_4$. Successively, the drying agent was removed via filtration through filter paper, and the resulting clear solution was collected in a round-bottom flask. The solvent was removed by rotavapor until purified cystamine (Cys), a pale-yellow viscous liquid, was obtained. The obtained Cys was then stored at -18 °C in a flask under an Ar atmosphere before its use.

Preparation of ESOA-Cys CANs

ESOA-Cys CANs were prepared by the direct combination of ESOA and Cys, taking into account the number of functionalities of the reactants, i.e., acrylate groups for ESOA and amino groups for Cys, respectively, as well as their reaction ratio. Considering that the amino group can react with one or two acrylic groups through Aza-Michael reaction, Cys was added according to Eq. 1 to obtain two different [acrylate]/[NH_2] ratios, i.e., 1:1 and 2:1 (Table 1).

$$m_C = \frac{MM_C}{MM_M} \times \frac{\upsilon_C}{\upsilon_M} = \frac{MM_C}{MM_M} \times \frac{\varphi_M}{\varphi_C} \quad (1)$$

Where: m_C is the crosslinker mass, MM_i is the molar mass of i, υ_i is the stoichiometric coefficient of i, and φ_i its functionality. The subscript C stands for the crosslinker (Cys), while the M stands for the matrix (ESOA). The obtained crosslinker mass is normalized to 1 g of matrix. For ESOA-Cys_1:1 $\varphi_c = 2$ and ESOA-Cys_2:1 $\varphi_c = 4$.

For the preparation of the ESOA-based CANs (**Fig. S1**), 1.00 g of epoxidized soybean oil acrylate (ESOA) was added to a vial, followed by Cys (90–180 µl). The resulting systems were mixed manually with a metal spatula for 2 min to ensure close contact between the reagents. The viscous and opalescent resins resulting from mixing were poured into silicone molds, and the entrapped air bubbles were removed by placing the molds under reduced pressure (10 mbar) for 3 min. The prepared formulations were then cured in an oven at 30, 50, or 100 °C for different times. The samples were coded according to their [acrylate]/[amino] ratio, the temperature, and the time used for the curing process, e.g., ESOA-Cys_2:1_50_48 denotes a sample with an [acrylate]/[amino] ratio of 2:1, which was cured at 50 °C for 48 h.

Characterization

Fourier-transform infrared spectroscopy (FT-IR) was performed using a Bruker® "Vertex 70" instrument, in ATR mode, single reflection, using a diamond crystal in the interval from 400 to 4000 cm^{-1}. All the FTIR spectra of the ESOA-Cys formulations were normalized with respect to the C=O stretching band at 1722 cm^{-1}. A direct proportional relationship between absorbance and concentration was assumed (Lamber-Beer law) to calculate the conversion using FT-IR spectra at different time points, and the following Eqs. 2 and 3 were used:

$$\text{Conversion}[\%] = \frac{A^0 - A(t)}{A^0} \cdot 100 \tag{2}$$

Where A^0 is the normalized initial area subtended to the acrylate peak between 793 and 822 cm^{-1}, and A(t) is the area at time = t.

$$\text{Conversion}[\%] = \frac{C^0 - C(t)}{C^0} \cdot 100 \tag{3}$$

Where C^0 is the initial area of the subtended area of the acrylate peak between 793 and 822 cm^{-1}, and C(t) the area at time = t, assuming $A^0 = C^0$ and A(t) = C(t) due to Lambert-Beer law.

^{1}H-NMR analysis was performed using a JEOL ECZ400R/S3®, operating at 400 MHz. The samples were dissolved in deuterated chloroform ($CDCl_3$) containing 0.03% v/v of tetramethylsilane (TMS) at a concentration of 20 mg/mL.

Thermogravimetric analysis (TGA) was performed using a Mettler Toledo TGA1 STARe System® instrument under dynamic and isothermal conditions. The dynamic experiments were carried out within a temperature range from 30 to 800 °C, using a heating rate of 10 °C/min and a nitrogen flow rate of 80 mL/min. In the case of isothermal measurements, the temperature was initially raised from 30 to 180 °C under nitrogen at a rate of 10 °C/min and then maintained at 180 °C for 2 h, switching the atmosphere from nitrogen to air while the flow rate remained the same.

Differential Scanning Calorimetry (DSC) of the materials was performed using a Mettler Toledo DSC1 STARe System®. The analysis was carried out using a three-step thermal program consisting of a first heating, a cooling, and a second heating in the temperature range between −130 and 30 °C for neat Cys and −100 °C to 50 °C for ESOA and the ESOA-Cys formulations. A heating/cooling rate of ±10 °C/min and a nitrogen flow rate of 20 mL/min were used for all steps.

The amount of crosslinked fraction and the density of crosslinks of the prepared formulations were determined by measuring the gel fraction (GF%) and the swelling ratio (SR%). To evaluate both GF% and SR%, individual specimens were weighed and immersed in 3 mL of toluene. This solvent was chosen for its ability to dissolve both ESOA and Cys. The swollen gels were weighed again after 3 days of immersion in the solvent and then vacuum dried for 24 h. The dried materials were weighed for a final time, and the GF% and SR% were calculated using Eqs. 4 and 5.

$$GF\% = \frac{m_d}{m_i} \times 100 \tag{4}$$

$$SR\% = \frac{m_s}{m_d} \times 100 \tag{5}$$

Where m_i is the initial mass, m_d is the dried gel, and m_s is the swollen gel.

Recycling tests were performed by manually shredding and hot pressing 1 g of material in a $30 \times 5 \times 0.5$ mm^3 copper mold at 180 °C for 20 min under a 2000 kg force.

Tensile tests of the prepared materials were performed using an Instron® mechanical tester, model 5565, on $30 \times 5 \times 0.5$ mm^3 samples using a strain rate of 0.2 mm/min.

The thermomechanical behaviour was determined by DMTA on a modular compact rheometer (MCR 702e MultiDrive, Anton Paar, Graz, Austria) in tensile mode. Rectangular-shaped specimens were tested in a temperature-sweep mode from −50 to 60 °C with a heating rate of 3 °C/min, an extensional strain of 0.1% (selected from the linear viscoelastic range), and a frequency of 1 Hz. To estimate the

apparent cross-linking density (ν_c), also referred to as strand density, the storage modulus in the rubbery plateau region (E'_R) was determined from the graph at approximately 40 °C above the α transition temperature. The value of ν_c was then calculated using Eq. 6. This equation originates from the statistical theory of rubber elasticity, which provides an approximate model of the system. Therefore, it was applied here solely for qualitative comparison of the relative crosslinking levels among the prepared networks.

$$\nu_c = \frac{E'_R}{3RT} \tag{6}$$

where ν_c is the number of moles of network chains per unit volume of the cured network, R is the gas constant equal to 8.314 J·K^{-1}·mol^{-1}, and T is T_α + 40 °C.

Rheological analysis of the materials was performed using an ARES plate-plate rheometer using 25 mm diameter disks (thickness = 1 mm) obtained by curing the formulations within silicone molds with suitable geometries, and storing the materials in a desiccator before analysis.

Stress relaxation tests were carried out using a modular compact rheometer (MCR 702e MultiDrive, Anton Paar, Graz, Austria) equipped with a parallel plate geometry. Samples were subjected to a constant stress of 0.5%, and the consequent strain level was monitored as a function of time. The storage modulus G(t) was normalized by the initial modulus G_0, and the characteristic relaxation time τ was determined as the time necessary to relax 1/*e* of the initial G_0 value.

Function fitting of the relaxation curves was performed using the Maxwell (Eq. 7) and the stretched exponential (Kohlrausch-Williams-Watts) (Eq. 8) model functions [40].

$$\frac{G(t)}{G_0} = Ae^{-\frac{t}{\tau}} \tag{7}$$

$$\frac{G(t)}{G_0} = Ae^{-(\frac{t}{\tau})^{\alpha}} \tag{8}$$

Where τ is the relaxation time, α is the stretched exponential factor, G(t) is the decay of the relaxation modulus at time t, and G_0 is the relaxation modulus at the initial time.

The activation energy E_a was calculated for each material by linear fitting of the relaxation times using an Arrhenius plot (Eq. 9).

$$ln(\tau) = \frac{E_a}{RT} - lnA \tag{9}$$

Where R is the gas constant equal to 8.314 J·K^{-1}·mol^{-1}, T is the absolute temperature, and A is the pre-exponential factor.

Enzymatic hydrolysis of the developed formulations was studied by placing 5 × 2 × 2 mm^3 samples (mean weight = 20 ± 2) inside a 1.5 mL Eppendorf containing 1 mL of 5 µM *Humicola insolens* Cutinase (HiC) (Novozym® 51.032) solution in potassium phosphate (KPO) 0.1 M buffer, pH = 8, which were then incubated at 50 °C. After the desired time, the remaining residues were carefully recovered, washed three times with milli-Q water, and then vacuum-dried at room temperature until constant weight was reached, before weight loss was determined gravimetrically on an analytical scale (± 0.00001 g).

Results and Discussion

The work focused on the preparation of formulations based on ESOA, i.e., a compound characterized by acrylate groups (average number per molecule = 3.4) that could potentially undergo an Aza-Michael reaction with the amino groups of Cys to form a covalent network.

To evaluate the effect of the reaction ratio on the final material properties, two formulations with different ratios of reactive acrylate to amino groups were prepared, namely 1:1 and 2:1, and their curing kinetics were monitored at increasing temperatures (30, 50, and 100 °C) over time.

Study of the Curing Reaction and Developed Materials

The Aza-Michael reaction (Fig. 2) between ESOA and Cys was verified and monitored by comparing the spectra of the starting materials with those of the formulations, over time, during the curing process (Fig. 3). The FT-IR spectrum of Cys (**Fig. S2**) displayed characteristic bands at 3360 and 3260 cm^{-1} (ν N-H stretching, symm. and asymm.), 2910 and 2892 cm^{-1} (ν C-H symm. and asymm.), as well as at 1590 cm^{-1} (δ N-H) as reported by other authors [41]. Moreover, the chemical structure and purity of the obtained Cys were further confirmed by ^{1}H-NMR analysis (**Fig. S3**). FT-IR analysis of ESOA (**Fig. S4**) revealed bands ascribed to specific vibrational motions at 3500 cm^{-1} (ν O-H), 2923

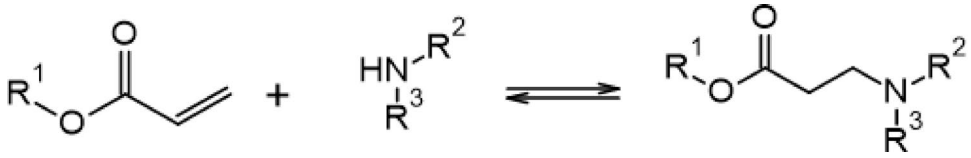


Fig. 2 Reaction scheme of Aza-Michael addition between an acrylic ester and a generic amine

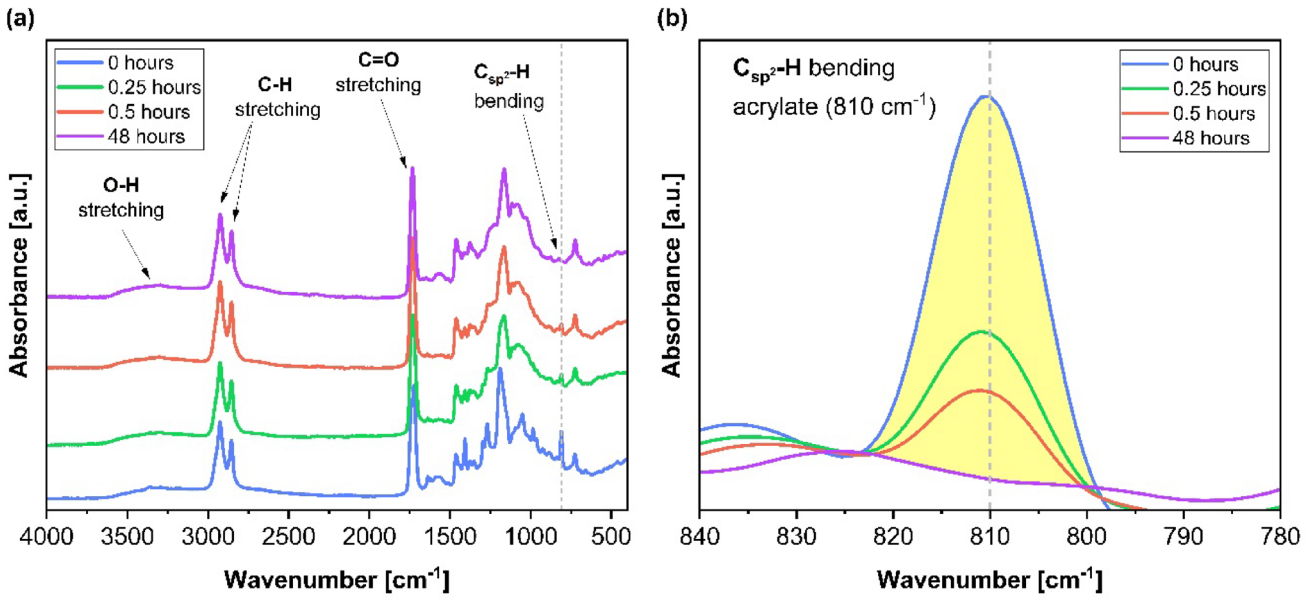


Fig. 3 Example of FT-IR spectra of ESOA-Cys_1:1 mixture (**a**) and zoom of its fingerprint region between 780 cm^{-1} and 840 cm^{-1} (**b**) at 100 °C and different curing times: 0 h (blue), 0.25 h (green), 0.5 h (red), and 48 h (purple)

and 2856 cm^{-1} (ν C_{sp3}-H asym. and symm.), 1722 cm^{-1} (ν C = O), 1633 cm^{-1} (ν C = C), and a diagnostic out-of-plane bending vibration of acrylates at 810 cm^{-1} (δ C_{sp2}-H acrylate) [3, 42, 43]. Similarly, the NMR spectrum of ESOA (**Fig. S5**) confirmed the expected structure. To monitor the extent of the Aza-Michael reaction between the acrylic groups of ESOA and the amino groups of Cys, the area under the signal associated with the acrylate moieties in the range 793–822 cm^{-1} was integrated over time (**Table S1** and **S2**).

The progressive decrease in the defined band area over time indicated that the reaction occurs with the consumption of acrylic double bonds, which is complete after a long reaction time (Fig. 3a and b). This decrement was accompanied by a concomitant reduction in the absorption peak at 1565 cm^{-1} associated with N-H bending of Cys, further supporting the effective reaction between the acrylate groups of ESOA and the amino moieties of Cys (**Fig. S6**). Moreover, in all the systems studied, a transition was observed from pourable mixtures with viscosity comparable to neat ESOA to rubbery, transparent materials over time, indicating network formation. It was also confirmed that the curing process is driven exclusively by the Aza-Michael reaction and not by undesired radical homopolymerization, as ESOA samples treated at the same temperatures and for the same duration showed negligible variations in acrylate concentration and viscosity.

Using the conversion data obtained from FT-IR analysis (**Fig. S7**, Table S1, and Table S2), the relative acrylate concentrations over time were calculated by applying Eqs. 2 and 3. These data were used to determine the curing kinetics for both ESOA-Cys_1:1 and ESOA-Cys_2:1, using a trial-and-error approach to identify the best-fitting kinetic model (e.g., first-order, second-order), as shown in Fig. 4. In particular, the best-fitting function for the ESOA-Cys_1:1 system was obtained by performing a linear fit of the integral function of the first-order kinetics over the entire conversion range (**Equation S1**).

In Fig. 4a, the fit lines, describing the curing kinetics of ESOA-Cys_1:1 at different temperatures, i.e., 30, 50, and 100 °C, exhibited the highest coefficients of determination ($R^2 > 0.96$) when pseudo-first-order kinetics was applied, indicating a good fit quality of the integral function used above (**Table S3**). In particular, the observed pseudo-first-order kinetics for ESOA-Cys_1:1 can be explained by considering an elementary reaction as shown in Fig. 4b, where a single acrylate group is expected to react with an amino group to form the corresponding β-aminoester. A similar trial-and-error approach was also applied to the ESOA-Cys_2:1 formulation (Fig. 4c). In this case, the fit of the integral function gave the best results ($R^2 > 0.92$) when correlated to a second-order reaction kinetics model (**Equation S2**), and only when performed at lower conversion values, i.e., below 60%, beyond which a noticeable change in the reaction regime occurs (**Fig. S8**). In the conversion range where a second-order reaction kinetics is followed, a reaction scheme involving two acrylate groups is expected to react with a single amino group to form a bis(β-amino ester) (Fig. 4d). As previously reported in the literature, the change of reaction regime can be explained by taking into account that, during the curing process, a significant increase in viscosity of the systems occurs, which can restrain molecular

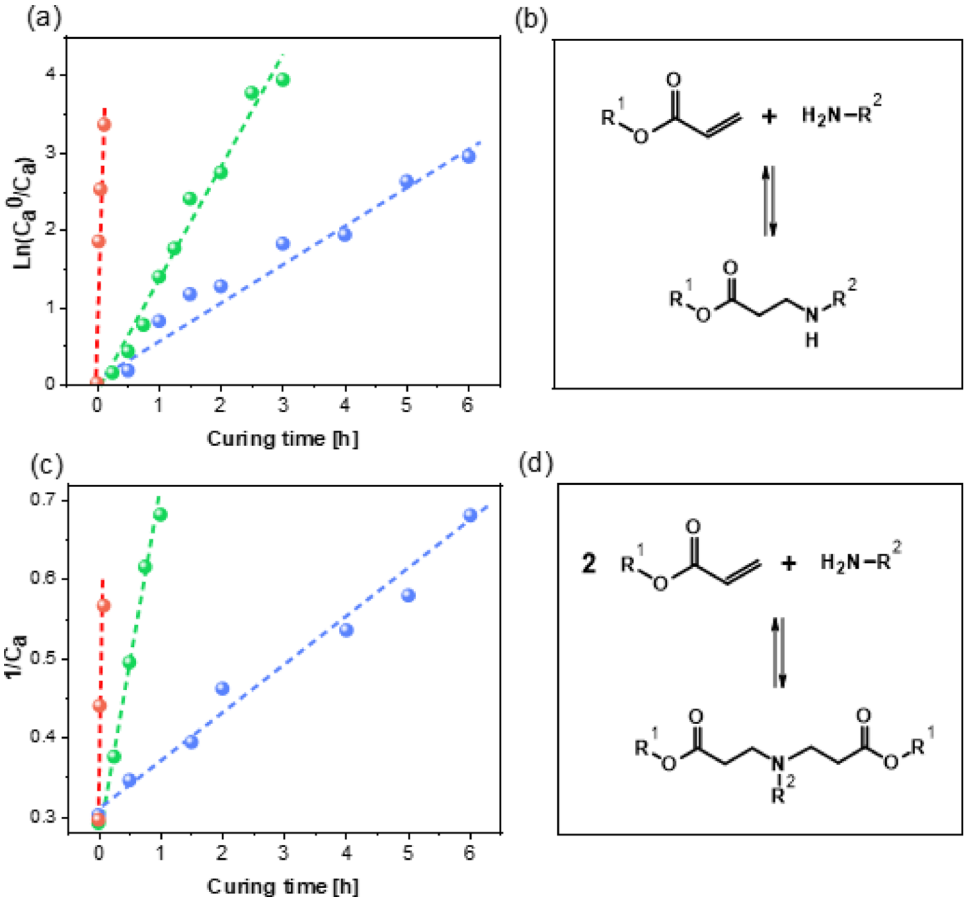


Fig. 4 Linear fits of the integral kinetic functions together with their corresponding reaction schemes for ESOA-Cys_1:1 (first-order, **a** and **b**) and ESOA-Cys_2:1 (second-order, **c** and **d**) at different temperatures: 30 °C (blue), 50 °C (green), 100 °C (red)

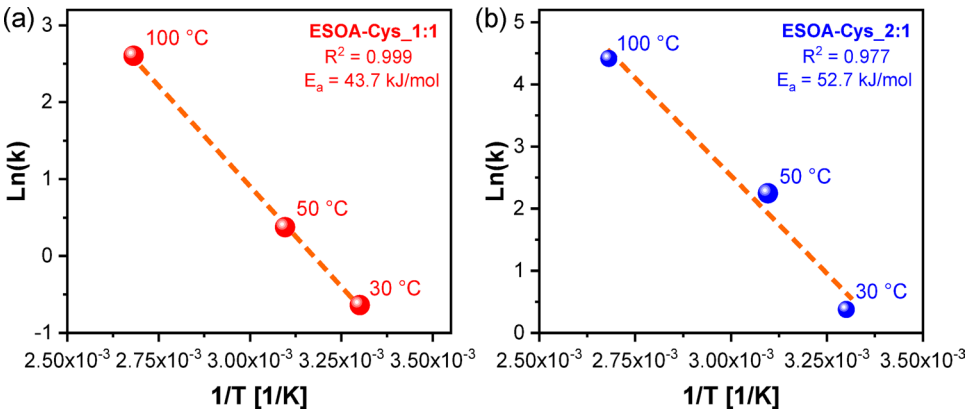


Fig. 5 Arrhenius plots of ESOA-Cys_1:1 (**a**) and ESOA-Cys_2:1 (**b**) formulations

mobility [44]. Another plausible explanation for the drop in reaction rate is the inability of the formed tertiary amines to further participate in the aza-Michael reaction. More specifically, when a secondary amine is converted to a tertiary amine, the system progressively loses available reaction sites, thus slowing down the overall curing process [45].

Moreover, the evaluation of the kinetic rate constants (*k*) (**Equation S3**), for the curing processes at various temperatures (30 °C, 50 °C, 100 °C), allowed the calculation of the activation energies (E_a) associated with the crosslinking processes of the two formulations (**Equation S4** and Fig. 5). Specifically, the activation energies were 43.7 kJ/mol and 52.7 kJ/mol for ESOA-Cys_1:1 and ESOA-Cys_2:1_100, respectively, with values consistent with those reported in the literature for curing processes based on the Aza-Michael reaction [45]. The slight difference in E_a can be attributed to the combination of processes that characterize network formation, which in turn depends on the different initial reactant ratios (Fig. 6).

Specifically, in the case of ESOA-Cys_1:1, Cys molecules can react with ESOA acrylate moieties through their two primary amino groups, forming β-aminoester bonds,

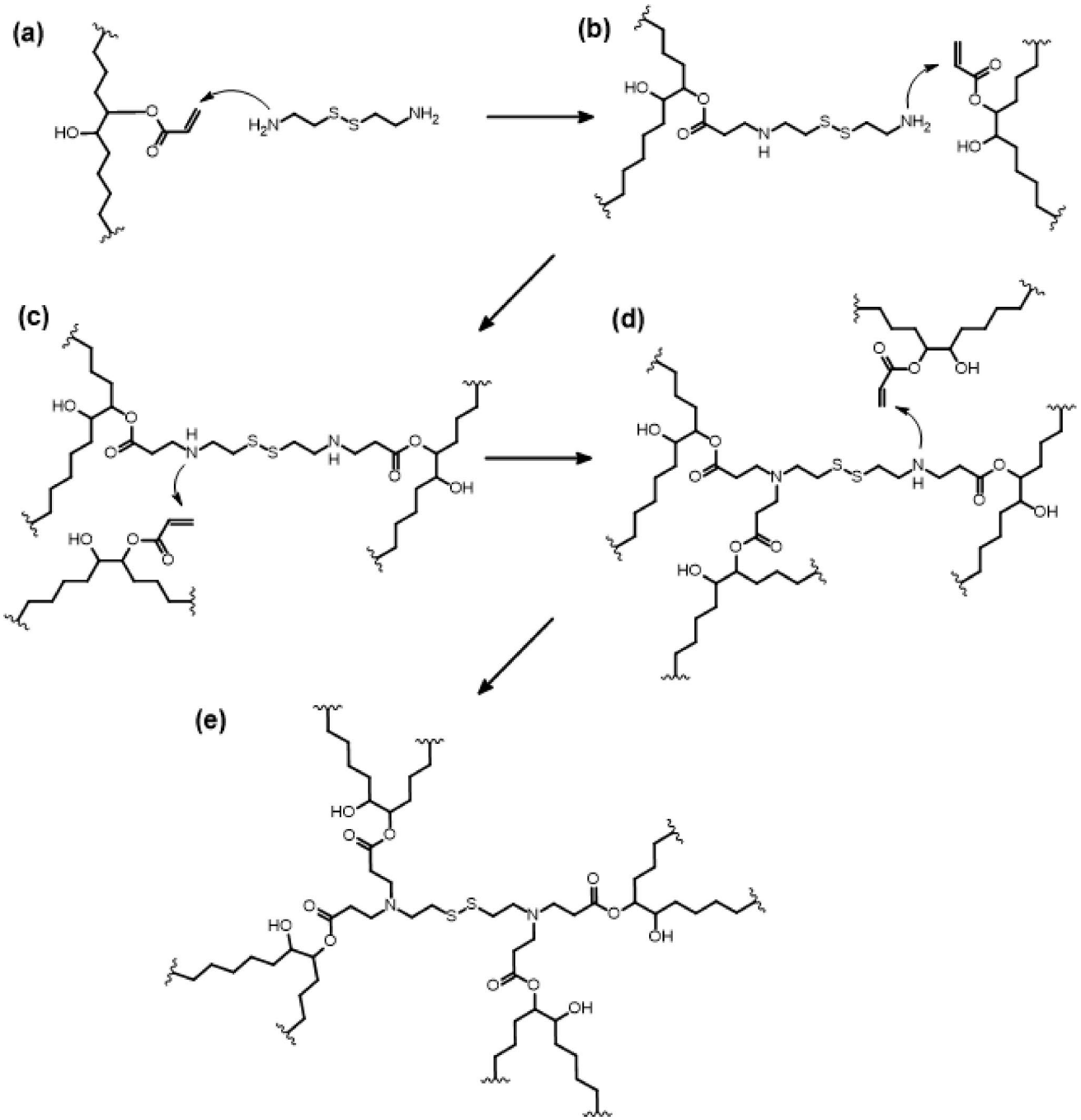


Fig. 6 Molecular scheme for the addition of Cys amino groups to ESOA during the curing process. Adducts deriving from the addition of Cys (**a**) to 1 (**b**), 2 (**c**), 3 (**d**), and 4 (**e**) molecules of ESOA

which can act as cross-links and convert the primary amines into secondary ones (steps a, b, and c in Fig. 6). The lower relative concentration of amine groups in ESOA-Cys_2:1 formulation favours a mechanism whereby the secondary amines (β-aminoesters) can further react with unreacted acrylate groups (steps d and e in Fig. 6). Indeed, for this formulation the reaction mechanism is more complex, involving two distinct steps, with the contribution of both primary and secondary amino reactions to form the corresponding β-amino esters [45]. However, it is possible to hypothesize that due to the steric hindrance of secondary amines, the corresponding reaction proceeds more slowly [46].

To provide evidence of the formation of a three-dimensional network, gel fraction (GF%) (Fig. 7) and swelling ratio (SR%) (Fig. 8) measurements were performed using

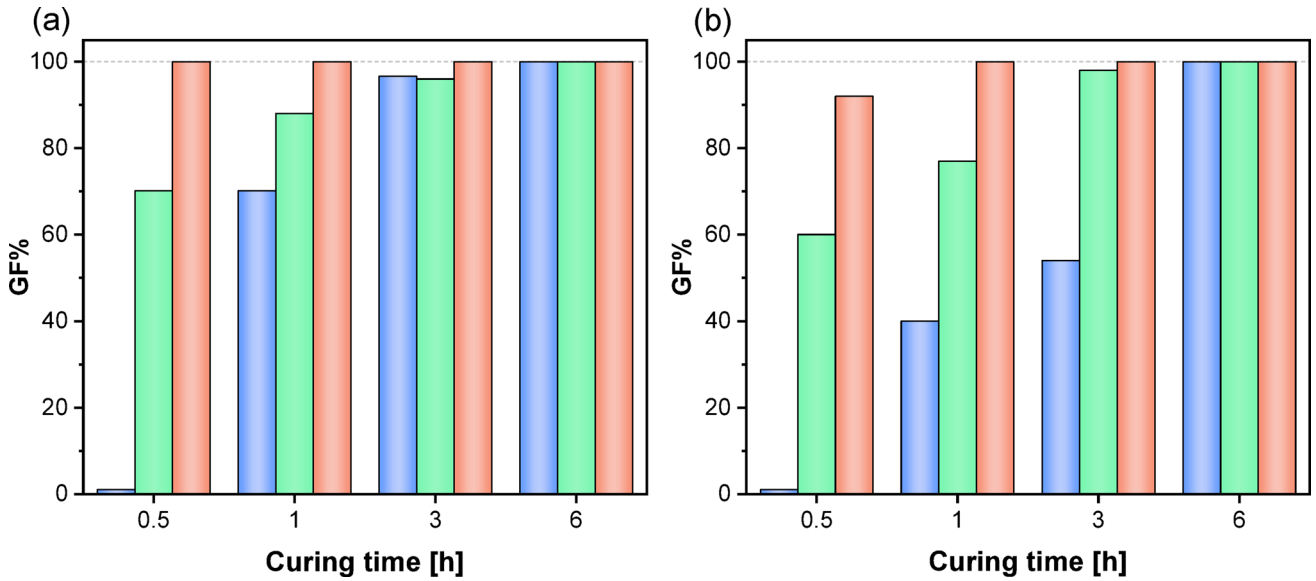


Fig. 7 GF% as a function of curing time for ESOA-Cys_1:1 (**a**) and ESOA-Cys_2:1 (**b**) formulations, at different temperatures: 30 °C (blue), 50 °C (green), and 100 °C (red)

toluene, i.e., a solvent capable of swelling the crosslinked fraction and dissolving both unreacted ESOA and Cys.

A direct comparison of the two systems under the same curing conditions showed that at shorter reaction times and lower temperatures, the formulations with a higher initial Cys content (ESOA-Cys_1:1) achieved higher GF% values than those with a lower Cys content (ESOA-Cys_2:1). Specifically, for both formulations, the GF% increased with both time and temperature, reaching complete crosslinking (GF% = 100) after 6 h under all temperature conditions tested. In the case of formulations cured at the highest temperature (100 °C), this time was reduced to 0.5 h for ESOA-Cys_1:1 and 1 h for ESOA-Cys_2:1. As previously highlighted, a possible explanation for this phenomenon is the faster kinetics of Aza-Michael additions with primary amino groups compared to secondary ones [45]. This phenomenon is also associated with the lower mobility of the latter groups formed during the curing process (Fig. 6), which are characterized by an increased steric hindrance and lower mobility when compared to primary ones. As already reported in the literature, this hindrance and the slightly higher reaction rates for primary amine in Aza-Michael addition of acrylates may justify the faster crosslinking observed in ESOA-Cys_1:1 samples [46]. Remarkably, the GF% values found for these systems are significantly higher than for other biobased CANs prepared using ESOA [30] or Cys [34, 47], highlighting the advantage of the proposed combination of ESOA and Cys.

The SR% analysis of both formulations, for samples with GF% values greater than 40%, under the tested curing conditions is given in Fig. 8. A decreasing trend of SR% over time was observed in all samples, stabilizing at a minimum plateau value after 24 to 48 h. Specifically, higher temperatures and Cys concentrations led to a faster decrease in SR% over time, reflecting the different curing kinetics found for the systems. In Fig. 9, the SR% of both formulations was compared after 48 h of curing at different temperatures, i.e., the time at which the minimum swelling was reached for each system.

The values measured for both formulations, when cured at the same temperature, were comparable, being 130%, 100%, and 60% for the systems cured at 30 °C, 50 °C, and 100 °C, respectively.

These low values, which indicate limited solvent uptake due to a dense polymer network, were found to be comparable to those typically found in similar systems, further highlighting the efficiency of the crosslinking process [48]. Interestingly, the plateau value observed in SR% was found to be independent of the ESOA/Cys molar ratio used and was hypothesized to be related to the limited molecular mobility and the depletion of reactive groups.

On the other hand, an increase in temperature promotes molecular diffusion and reactive segments mobility, enhancing network density and reducing the swelling ratio of materials. These results highlight that the limit in the cross-linking process is not only determined by the concentration of reactive groups but also by the viscosity, which directly affects their diffusive capacity and configurational entropy, leading to a transition from chemical-kinetic control to diffusive regime. Overall, these results confirm that the proposed bio-based reactants can be effectively crosslinked even under mild conditions and demonstrate not only the efficiency of Cys as a suitable biobased cross-linker for acrylate-functionalized compounds, but also the critical role

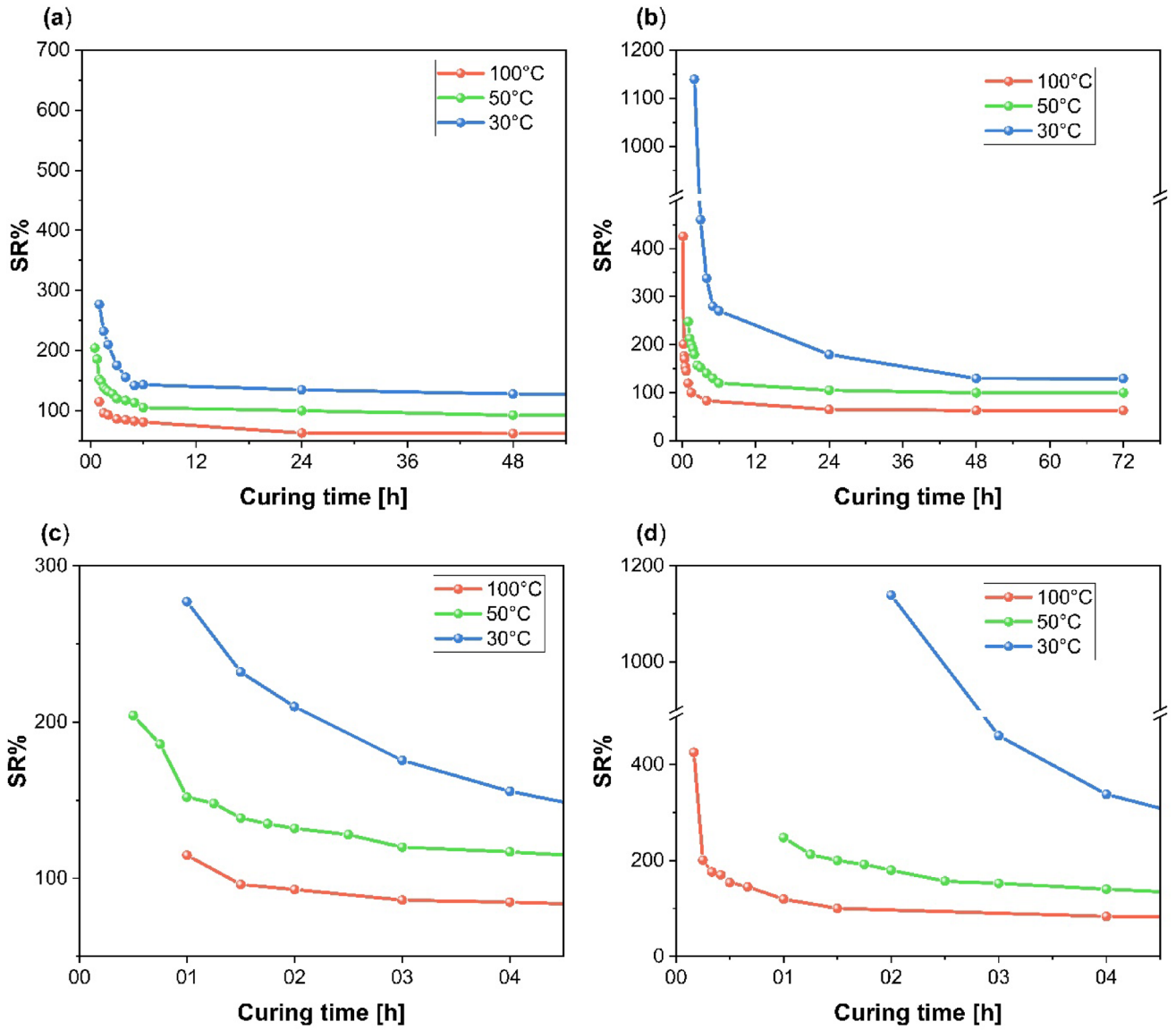


Fig. 8 SR% as a function of curing time for ESOA-Cys_1:1 (**a**) and ESOA-Cys_2:1 (**b**) at 30 °C (blue), 50 °C (green), and 100 °C (red), zoomed graphs of initial times for curing of ESOA-Cys_1:1 (**c**) and ESOA-Cys_2:1 (d)

of monomer/crosslinker stoichiometry in determining the optimal curing conditions.

DSC analysis was used to characterize the starting materials and further study the curing process of ESOA-Cys formulations. The thermogram of neat ESOA showed a T_g of -39 °C with the additional presence of broad cold crystallization (T_{cc}) and melting (T_m) transitions occurring at -15 °C and 4 °C, respectively (**Fig. S9**). Similarly, Cys was characterized by comparable thermal transitions, exhibiting a T_g of -96 °C and cold crystallization and melting processes at -61 °C and −25 °C, respectively (**Fig. S10**). To study the evolution of the cross-linking process, DSC traces of the two formulations were recorded over time, curing the samples at 100 °C, i.e., at the temperature characterized by the fastest kinetics among the temperature treatments investigated (**Fig. S11**). The thermogram of the initial mixture (t = 0) showed the characteristic peaks of the cold crystallization and melting transitions described for neat ESOA. On the other hand, the thermal transitions associated with Cys were not observed. This result can be attributed to the formulation preparation procedure, which consisted of mixing the two reagents at room temperature for 2 min to ensure intimate contact, followed by 3 min of degassing under vacuum. This procedure should provide sufficient time to initiate the crosslinking process, which can occur even at room temperature and causes Cys to react, explaining the absence of its characteristic thermal events. The starting T_g for both ESOA-Cys_1:1 and ESOA-Cys_2:1 mixtures was −35 °C,

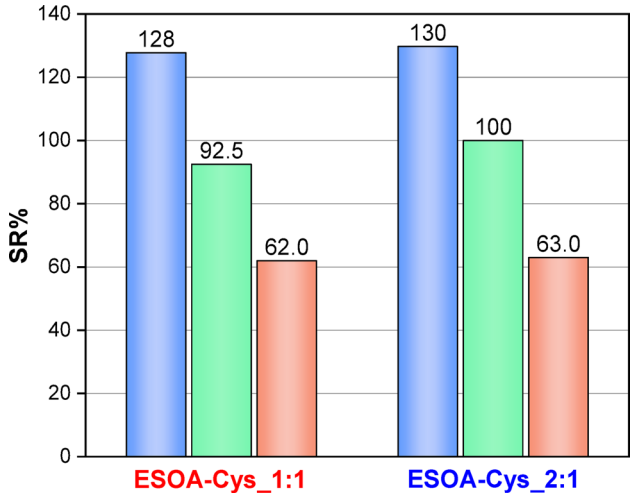


Fig. 9 SR%, after 48 h of curing, of the two formulations cured at 30 °C (blue), 50 °C (green), and 100 °C (red)

higher than the value calculated using the Flory-Fox equation for the starting systems (-48 °C and −44 °C for 1:1 and 2:1, respectively), a phenomenon which can be explained by considering the above-mentioned cross-linking reaction during the mixing step. Interestingly, the T_g of the formulations was found to gradually increase over time during the curing process, with a faster increase observed for the 1:1 system, in accordance with the different reaction kinetics (Fig. 10). After 0.66 h (40 min) of curing, both formulations reached comparable T_g values, of -3 °C and −4 °C for 1:1 and 2:1, respectively, which levelled off to the same value of -2 °C after 2 days (**Fig. S12**).

Table 2 TGA of starting materials and ESOA-Cys mixtures

Sample	T_{onset} (°C)		T_{max}*(°C)
Cys	186		209
ESOA	294		363
Sample	T_{onset} (°C)	T_{maxI}*(°C)	T_{maxII}*(°C)
ESOA-Cys_1:1_100_48	225	258	394
ESOA-Cys_2:1_100_48	234	256	385

*: extrapolated from DTG data

These findings, which are consistent with the formation of crosslinks within the systems, confirm the effectiveness of the curing time used for sample preparation.

The comparison with other works in the literature dealing with ESOA-based materials deserves a detailed comment. For example, Coste et al. developed soft ESOA-based foams by crosslinking this compound with various diamines in bulk, using a 2:1 molar ratio of amino to acrylate. In these systems, complete crosslinking was demonstrated by the disappearance of the acrylate signal in FTIR spectra after a curing process of 4 h at 50 °C, followed by 2 h at 120 °C [49]. The much faster curing process, which characterizes our systems, demonstrates the rapidity of the Aza-Michael reaction, which ensures complete crosslinking under mild conditions. This underlines the sustainability of the developed materials not only because the starting components are derived from renewable raw materials, but also because of the simple scale-up process.

TGA/DTG measurements (**Fig. S13** and Table 2) were performed to evaluate the thermal stability of the starting materials and the formulations with the highest cross-linking

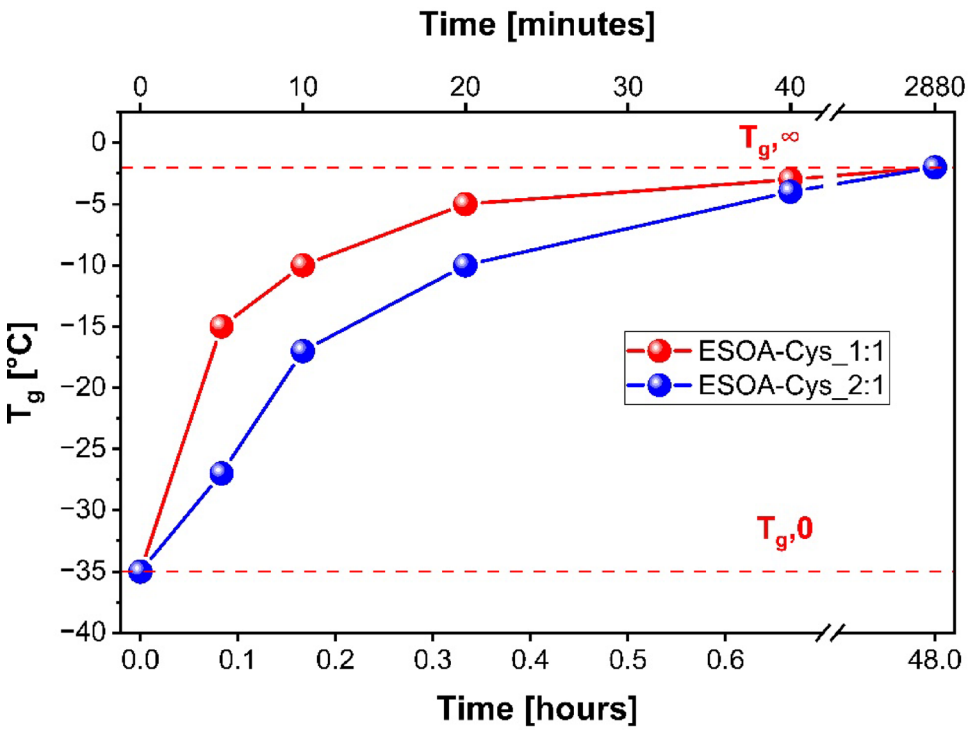


Fig. 10 T_g values of ESOA-Cys_1:1 (red) and ESOA-Cys_2:1 (blue) mixture over time, when cured at 100 °C

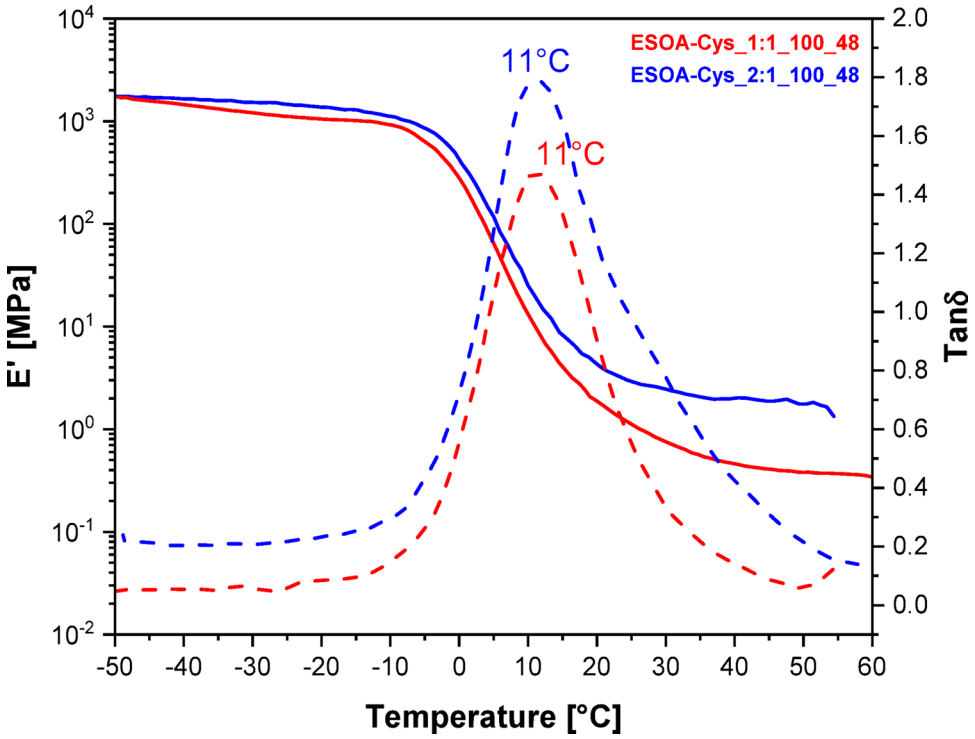


Fig. 11 DMTA curves for ESOA-Cys_1:1_100_48 and ESOA-Cys_2:1_100_48: E' (solid lines) and tanδ (dashed lines)

density, specifically those cured at 100 °C for 48 h, defined as ESOA-Cys_1:1_100_48 and ESOA-Cys_2:1_100_48. The analysis of ESOA exhibited a single-step decomposition process, characterized by an initial weight loss temperature (T_{onset}) of 300 °C and a maximum volatilization rate temperature (T_{max}) of 363 °C, in perfect agreement with previously reported data for this material [50]. Analogously, Cys showed a single-step volatilization process characterized by lower T_{onset} and T_{max} values of 186 °C and 209 °C, respectively. A direct comparison with literature data was not possible for this compound, as no thermogravimetric data were found for Cys free base. However, its salts exhibited T_{onset} values in the range of 210–220 °C, which were attributed to the homolytic cleavage of the S-S bond occurring at approximately 200 °C [51, 52].

The TGA curves of the crosslinked materials displayed a two-step degradation profile characterized by an initial, slight mass loss at 220–240 °C, followed by a more pronounced weight loss at 390 °C. This behavior was attributed to the sequential decomposition of the components within the network. In particular, for both formulations, the first thermal event (T_{maxI}) at 260 °C was assumed to be related to the degradation and volatilization of the Cys fraction [53] while the second one (T_{maxII}) at 390 °C was associated with the decomposition of the ESOA fraction [54]. Moreover, a direct comparison between the two systems revealed a slightly higher T_{onset} of ESOA-Cys_2:1_100_48 (234 °C vs. 225 °C), suggesting that the higher crosslinking density delays the release of volatile products. Higher thermal stability of ESOA-Cys_2:1_100_48 was also confirmed under isothermal conditions at 180 °C (**Fig. S14**). The thermal stability of these systems proves to be comparable to that of soft foams prepared via Aza-Michael reaction between ESOA and aliphatic (cadaverine) or aromatic (MXDA) diamines, demonstrating that the presence of an additional dynamic S–S bond does not negatively affect this property [49].

Table 3 Thermomechanical properties of ESOA-Cys samples

Sample	T_α [°C]	E'_G [MPa]	E'_R [MPa]	ν_c [mol/dm^3]
ESOA-Cys_1:1_100_48	11	1700	0.2	0.03
ESOA-Cys_2:1_100_48	11	1876	1.3	0.16

The thermomechanical properties of the cured samples were evaluated by DMTA measurements. As shown in Fig. 11, only minor differences in the elastic modulus in the glassy region at low temperature were observed between the materials. In contrast, the modulus at the plateau in the rubbery region, known as rubbery modulus (E'_R), was higher for ESOA-Cys_2:1_100_48 compared to ESOA-Cys_1:1_100_48 (Table 3), suggesting the formation of a more rigid network [55]. The rubbery modulus, which is related to the crosslinking density (ν_c) of the thermosetting network, indicates a higher ν_c for ESOA-Cys_2:1_100_48 compared to ESOA-Cys_1:1_100_48, which led to a broadening of the Tanδ curve. These results also suggest the presence of a complex network behavior, based on a wider distribution of chain mobility within the network [56, 57]. However, the peak temperature of the tanδ, representing the

main relaxation α, was at 11 °C for both formulations, in good agreement with the glass transition temperatures measured by DSC.

To further investigate the viscoelastic behavior at high temperature, frequency sweep tests in a plate-plate rheometer were carried out at 180°C (**Fig. S15**). ESOA-Cys_2:1 exhibited an elastic shear modulus (G') higher than the loss modulus (G'') over the whole frequency range, confirming its crosslinked nature even at high temperature. An elastic plateau was observed for frequencies down to 10^{-1} rad/s, while at lower frequencies (*i.e.*, longer times), a slight decrease was noted, which was interpreted as a slow chain relaxation phenomenon. ESOA-Cys_1:1_100_48 also showed elastic-dominated behavior for frequencies higher than 10^{-1} rad/s. However, a crossover between G' and G'' was observed at 0.014 rad/s, indicating that the network relaxation in this system was significantly faster for the lower crosslinking density network. This difference was attributed to the higher concentration, in ESOA-Cys_1:1_100_48, of groups capable of participating in dynamic exchange processes, promoting network rearrangements as commonly reported for CANs [58].

To investigate the network dynamics over extended periods, stress relaxation experiments were carried out. Both formulations exhibited complete relaxation within a few hours at 170 °C (Fig. 12), which was taken as the maximum temperature to avoid potential degradation of the network, according to the thermal stability evaluated under isothermal conditions (Fig. S14). At lower temperatures, consistent plots were obtained, although complete relaxation was not observable due to practical limitations in the test duration. The stress relaxation plots exhibited different profiles depending on the ESOA-Cys ratio. ESOA-Cys_2:1_100_48 relaxation followed the typical profile for covalent adaptable networks, with an initial slow stress decrease over time [59]. On the contrary, the formulation ESOA-Cys_1:1_100_48 showed a much faster decay of the modulus at the beginning of the test, consistent with the relaxation of a system with a lower crosslinking density (Table 3). Fitting the stress-relaxation plots by the Maxwell model, previously proposed for some dynamic polymer networks [60], was found unsatisfactory for both ESOA-Cys_1:1_100_48 and ESOA-Cys_2:1_100_48 (Fig. 12a and c). In contrast, fitting with "stretched" exponential decay functions $\frac{G(t)}{G_0} = Ae^{-\left(\frac{t}{\tau}\right)^{\alpha}}$ provided quite accurate fitting for ESOA-Cys_2:1_100_48 (Fig. 12b and d), whereas for ESOA-Cys_1:1_100_48 only the relaxation plots obtained at the highest temperatures (170 and 165 °C) were satisfactorily fitted by the same function (Fig. 12b). Specifically, the α values indicate the width of the relaxation time distribution, with lower α values associated to more heterogeneous segment dynamics [40]. This model was previously applied to other dynamic networks with low crosslinking densities, and the $\alpha < 1$ exponent was correlated with the possibility of additional relaxation

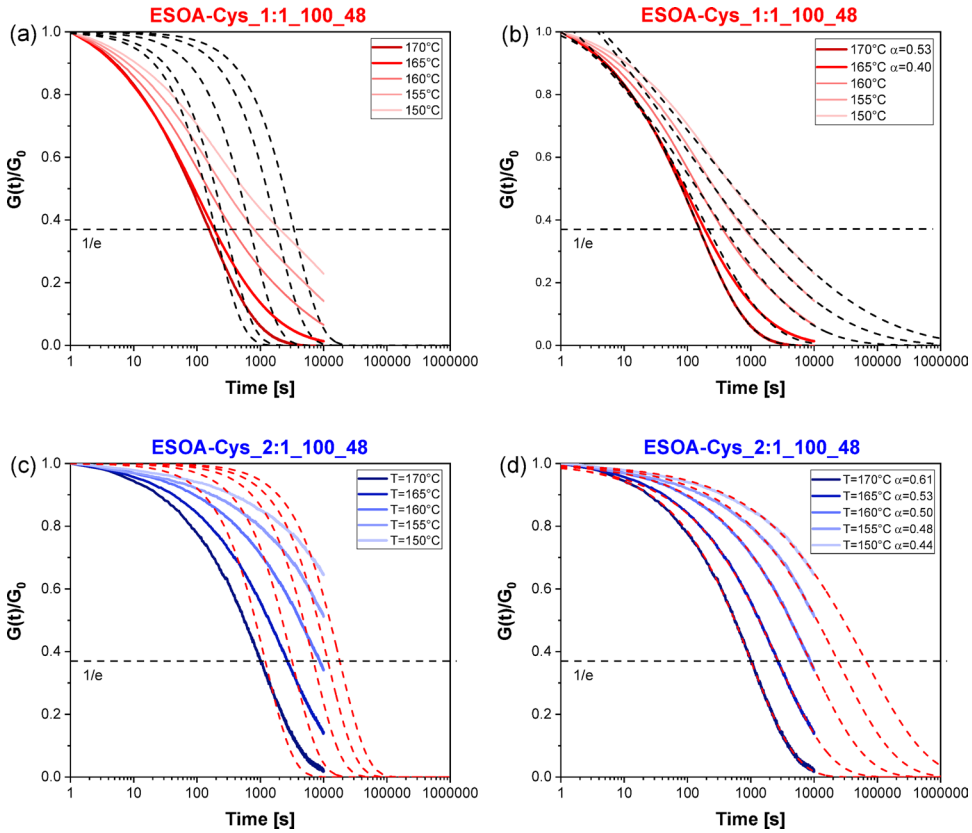


Fig. 12 Stress-relaxation curves of ESOA-Cys formulations fitted with Maxwell (**a** and **c**) and stretched exponential decay (**b** and **d**) model functions

modes, beside bond exchange within the networks [61, 62]. In ESOA-Cys_2:1_100_48, α values of 0.5 ± 0.1 were obtained (Fig. 12d), with an apparent slight decrease as temperature decreased. However, α values obtained from partial relaxation plots at lower temperatures, as already reported, may be affected by a significant error, indicating that the results achieved at different temperatures may be equivalent. For ESOA-Cys_1:1_100_48, representative α values could be obtained only at high temperature, in the same range as for ESOA-Cys_2:1_100_48. At lower temperature, the stretched exponential model is not satisfactory to account for the relaxation in the short time range, reflecting a more complex relaxation process. Assuming a (stretched) exponential decay for stress-relaxation as an approximate solution for both formulations, a characteristic relaxation time (τ) can be derived from the 1/e threshold on the $\frac{G(t)}{G_0}$ plots (Fig. 12). Plotting these relaxation times vs. inverse temperature (Fig. 13) confirmed the Arrhenius dependence of the relaxation process, allowing to calculate the activation energy (E_a) of the relaxation for the two networks. For ESOA-Cys_1:1_100_48, the Arrhenius fit is very good at temperatures ≤ 165 °C, yielding E_a of ca. 245 kJ/mol. This activation energy is in good agreement with values previously reported for β-amino ester-based networks by du Prez and co-workers up to 242 kJ/mol [35]. While the metathesis of disulfide bonds may also contribute to network rearrangement [63], based on the obtained activation energy we attribute the network rearrangement to retro-aza-Michael exchange. Interestingly, the experimental point at 170 °C is significantly out of the linear fitting, which may suggest a transition between different exchange mechanisms in the network, due to the activation of an independent chemical process. For ESOA-Cys_2:1_100_48, relaxation times (**Table S4**) are at least one order of magnitude higher, compared with ESOA-Cys_1:1_100_48 at each relaxation temperature. This reflects the slower dynamics related to the formation of tertiary amines as a consequence of the different initial reactant ratios, yielding an activation energy for the network relaxation at 343 kJ/mol. Overall, these results highlight the greater sensitivity of the thermomechanical analyses to differences in network topology, compared to the other characterization methods used in this study, namely thermal analysis and swelling ratio measurements.

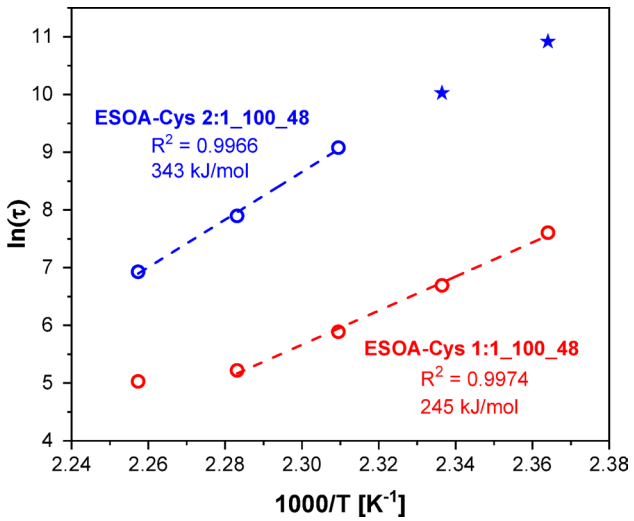


Fig. 13 Arrhenius plot for ESOA-Cys formulations. Star-shaped points represent extrapolated relaxation times based on stretched exponential fitting of relaxation curves beyond the explored time range. These points were not considered for the Arrhenius fitting and were reported only to demonstrate the linearity of the fitting, even at lower temperatures

Recyclability and Self-Healing Test

To assess the recyclability of the developed systems, recycling tests were carried out with both ESOA-Cys systems at different temperatures. Specifically, the specimens were cut into small fragments and placed in rectangular molds that were preheated for 3 min to soften the material, then pressed at the desired temperature (160 °C, 170 °C, or 180 °C) for 20 min under a 2-ton load (**Fig. S16**). These temperatures were chosen based on the results of stress-relaxation tests to ensure sufficient bond exchange and interdiffusion kinetics among the macromolecular segments, allowing the molding within a short time frame.

For both systems, the samples obtained after hot pressing at 160 °C and 170 °C showed visible defects and voids, indicating poor interparticle adhesion within the applied processing time. This was probably caused by slow network dynamics at these temperatures, in agreement with the stress-relaxation analysis (Fig. S14). In contrast, processing at 180 °C produced homogeneous, transparent films comparable to the original samples, demonstrating the effectiveness of these conditions for recycling these formulations via compression molding.

To further assess the thermomechanical stability of the materials during recycling, properties such as Young's modulus, GF%, and elongation at break were monitored as a function of the number of hot-pressing cycles (Table 4). For both systems, Young's modulus (E) and ultimate strength progressively decreased after each reprocessing cycle, reaching a plateau value after the second cycle. This reduction in properties coincided with a drop in GF%, which dropped from 100% for the pristine samples to 79% and 88% for the 1:1 and 2:1 formulations, respectively, after the third cycle, with the 1:1 system showing the most pronounced reduction. Conversely, the elongation at break increased after each cycle for both formulations, generally being higher for ESOA-Cys_1:1_100_48, in agreement with the described differences in network topology. This increase could be attributed to the gradual accumulation of

Table 4 Mechanical properties and gel fraction values of the ESOA-Cys formulations before and after several hot-pressing cycles

System	Cycle	Young's modulus (MPa)	Ultimate strength (MPa)	Elongation at break (%)	GF (%)
ESOA-Cys_1:1_100_48	0	4.3±0.5	0.35±0.05	23.0±2.2	100
	1	2.3±0.2	0.16±0.03	27.7±2.4	92
	2	1.1±0.1	0.12±0.02	31.0±2.5	86
	3	1.0±0.1	0.11±0.03	35.0±2.9	79
ESOA-Cys_2:1_100_48	0	3.4±0.3	0.35±0.05	9.20±0.1	100
	1	2.1±0.1	0.27±0.05	15.0±0.8	94
	2	1.4±0.1	0.24±0.04	20.9±0.8	90
	3	1.4±0.1	0.24±0.05	25.5±0.9	88

a non-crosslinked, soluble fraction that acts as an internal plasticizing component within the networks. As reported by other authors, this effect can be attributed to several factors, such as the breaking of covalent bonds during grinding [64], changes in network topology, and side reactions [65] such as hydrolysis or oxidation [66]. In our system, it is possible to hypothesize that the formation of the soluble fraction may be due to chain scission, with degradation not related to the formation of volatile products, as highlighted by TGA analysis. The self-healing test was carried out similarly by cutting a 1 × 25 mm rheology sample into two parts, which were then brought into contact at 180 °C, the same temperature at which homogeneous specimens were produced via compression moulding (**Fig. S17**). Ideal contact between the cut sample edges was achieved by fixing the sample and placing a glass slide on top to avoid specimen movements. After 0.5 h of heating, an uninterrupted film with no visible marks was obtained, demonstrating that the conditions used were sufficient to ensure good adhesion between the different pieces. Interestingly, the observed recyclability and self-healing performance of the developed CANs were comparable to those of other systems reported in the literature based on the same type of exchange reactions [37]. It is also important to highlight that the stabilization of the studied parameters after the second recycling demonstrates the suitability of the developed formulations for real recycling applications where material stability over several reprocessing cycles is required. These features, introduced by multiple bond-exchange modalities, make these materials easily mouldable and effectively recyclable in a short time without catalysts.

Enzymatic Hydrolysis

The enzymatic hydrolysis of films was investigated, focusing on the biobased nature of the components to provide a sustainable end-of-life strategy for the formulated materials and to assess their potential biodegradability (Fig. 14). Specifically, the stability of the crosslinked systems was evaluated under controlled conditions by using *Humicola insolens* cutinase (HiC) solution in KPO 0.1 M pH = 8, with samples incubated at 50 °C. This enzyme, known for its high hydrolytic activity towards many aliphatic polyesters, was chosen due to the presence of ester groups in the triglyceride structures within ESOA, which can be potential substrates for HiC. In detail, the hydrolysis of the formulations, prepared with two different ESOA/Cys ratios (ESOA-Cys_1:1_100_48 and ESOA-Cys_2:1_100_48), showed comparable mass loss trends over time, with complete dissolution of the specimens after approximately 60 days (1440 h).

These results suggest that the degradation kinetics of these systems were not significantly affected by the amount of Cys used or by the associated differences in crosslinking

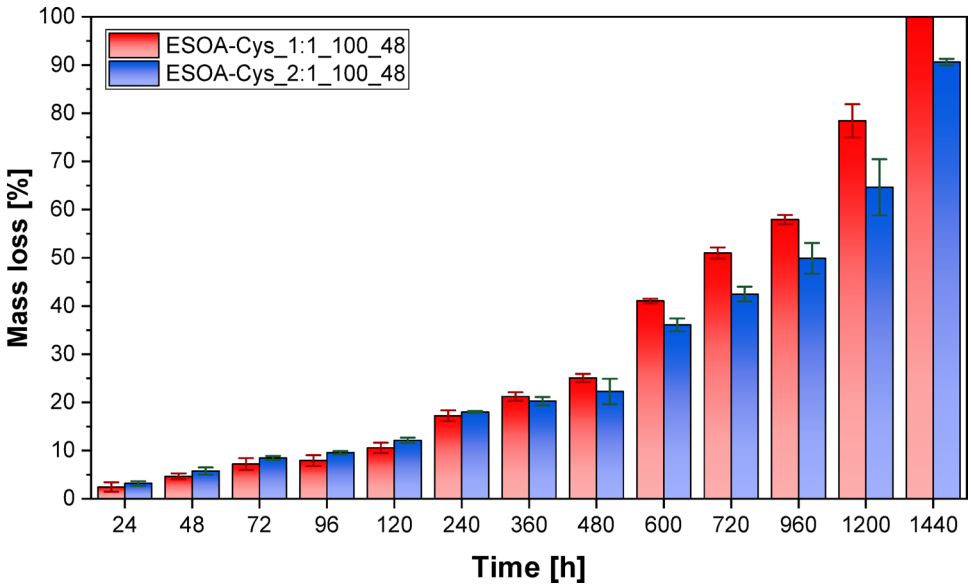


Fig. 14 Enzymatic hydrolytic degradation profile of ESOA-Cys_1:1 (red) and ESOA-Cys_2:1 (green) in 5 µM HiC solution in 0.1 M KPO buffer pH = 8

density observed between samples cured at 100 °C. Additionally, the active role of HiC in the degradation process was confirmed by placing control samples in the medium without the enzyme, i.e., KPO buffer pH = 8, showing negligible mass loss after 60 days. However, direct comparison of these results with the current literature is challenging, as this is the first time HiC has been used to promote the hydrolysis of crosslinked triglycerides, whereas in other studies, ESOA-based materials have generally been hydrolyzed using other enzymes belonging to the hydrolase class. For example, Sibilia et al. investigated the enzymatic hydrolysis of ESOA-based scaffolds using lipase from *Candida rugosa*, an enzyme with comparable activity towards ester bonds [67]. In another work, crosslinked ESOA microparticles obtained via photocuring were subjected to enzymatic hydrolysis using an esterase and a lipase [68]. These findings also highlight the specific role of the crosslinked network in hydrolysis time, as linear systems characterised by ester functionalities, such as PLA [69] or PCL [70], can be completely hydrolysed within a few days, compared with 60 days for the developed formulations. Nevertheless, these encouraging results highlight the potential biodegradability of the ESOA-Cys systems and demonstrate the applicability of HiC to develop novel chemo-enzymatic recycling strategies for crosslinked triglyceride-based systems.

Conclusions

This work demonstrates the feasibility of producing covalent adaptable networks (CANs) from bio-based reagents, namely epoxidized soybean oil acrylate (ESOA) and cystamine (Cys), under mild conditions and in the absence of catalysts or solvents. Such reactivity arises from the distinctive functional groups present in Cys and ESOA, which readily undergo an Aza–Michael addition. The novelty of this study lies not only in the choice of bio-based precursors but also in the approach adopted to investigate network formation, which revealed the presence of distinct kinetic regimes governed by the reagent ratio. In particular, for the formulation based on a ratio of ESOA and Cys 1:1 (ESOA-Cys_1:1), Cys molecules reacted with ESOA acrylate groups through their two primary amines, forming β-amino ester linkages that acted as crosslinks while converting the primary amines into secondary amines. In contrast, in the formulation with a lower relative concentration of amine groups (ESOA-Cys_2:1), the subsequent reaction of the newly formed secondary amines with residual acrylate groups was further promoted. This difference influenced the curing kinetics, with ESOA-Cys_1:1 reaching complete cross-linking more rapidly than ESOA-Cys_2:1, owing to the higher reactivity of primary amines in Aza-Michael addition reactions compared to secondary amines. Both formulations exhibited complete stress relaxation within a few hours at 170 °C. However, while ESOA-Cys_2:1 cured at 100 °C for 48 h displayed the characteristic relaxation behaviour of covalent adaptable networks, with an initially slow decrease in stress over time, ESOA-Cys_1:1_100_48 showed a markedly faster initial decay of the relaxation modulus. This behaviour is consistent with the relaxation response of a network characterized by a lower crosslink density.

Overall, the developed CANs combine several advantageous features, including tunable properties achieved through simple adjustment of the reagent ratio, recyclability, degradability via enzymatic hydrolysis, the bio-based origin of the reagents, and a simple, scalable preparation process. These characteristics highlight the potential of these materials for future practical and sustainable applications.

Supplementary Information The online version contains supplementary material available at https://doi.org/10.1007/s10924-026-03915-2.

Acknowledgements Funded by Fondazione Compagnia di San Paolo within the framework of the Obiettivo Pianeta call (contribution #17277) and ERC CIRCULARIZE (101114664) (European Union). Views and opinions expressed are, however, those of the author(s) only and do not necessarily reflect those of the European Union or the European Research Council. Neither the European Union nor the granting authority can be held responsible for them.

Author Contributions All authors contributed to the study conception and design. Material preparation, data collection and analysis were performed by Leonardo Giribaldi, Giacomo Damonte and Camilla Noè. The first draft of the manuscript was written by Leonardo Giribaldi and Giacomo Damonte and all authors commented on previous versions of the manuscript. All authors read and approved the final manuscript.

Funding Open access funding provided by Università degli Studi di Genova within the CRUI-CARE Agreement.

Data Availability No datasets were generated or analysed during the current study.

Declarations

Competing Interests The authors declare no competing interests.

Open Access This article is licensed under a Creative Commons Attribution 4.0 International License, which permits use, sharing, adaptation, distribution and reproduction in any medium or format, as long as you give appropriate credit to the original author(s) and the source, provide a link to the Creative Commons licence, and indicate if changes were made. The images or other third party material in this article are included in the article's Creative Commons licence, unless indicated otherwise in a credit line to the material. If material is not included in the article's Creative Commons licence and your intended use is not permitted by statutory regulation or exceeds the permitted use, you will need to obtain permission directly from the copyright holder. To view a copy of this licence, visit http://creativecommons.org/licenses/by/4.0/.

References

1. Mariani A, Malucelli G (2025) Biobased vitrimers: towards sustainability and circularity. Chem Commun. https://doi.org/10.1039/D4CC05967K
2. Sun M, Felsenthal LM, Kim S, Choi EY, Reed LJ, Elling BR, Dichtel WR (2026) Covalent adaptable networks: reprocessable cross-linked polymers. Chem Rev. https://doi.org/10.1021/acs.chemrev.4c00994
3. Damonte G, Pellis A, Battegazzore D, Athanassiou A, Zych A, Fina A, Monticelli O (2024) On sustainable vitrimers based on polycaprolactones. ACS Appl Polym Mater. https://doi.org/10.1021/acsapm.3c03192
4. Ferretti F, Damonte G, Cantamessa F, Arrigo R, Athanassiou A, Zych A, Fina A, Monticelli O (2024) On a biobased epoxy vitrimer from a cardanol derivative prepared by a simple thiol-epoxy click reaction. ACS Omega. https://doi.org/10.1021/acsomega.3c07459
5. Manarin E, Da Via F, Rigatelli B, Turri S, Griffini G (2023) Biobased vitrimers from 2,5-furandicarboxylic acid as repairable, reusable, and recyclable epoxy systems. ACS Appl Polym Mater. https://doi.org/10.1021/acsapm.2c01774
6. Stewart KA, Lessard JJ, Cantor AJ, Rynk JF, Bailey LS, Sumerlin BS (2023) High-performance polyimine vitrimers from an aromatic bio-based scaffold. RSC Appl Polym. https://doi.org/10.1039/D3LP00019B
7. Stewart KA, Le TH, Wei NB, Cantor AJ, Rynk JF, Sumerlin BS (2024) Biobased polystyrene vitrimers for thermoset circularity. ACS Appl Polym Mater. https://doi.org/10.1021/acsapm.4c01900
8. Sangaletti D, Ceseracciu L, Marini L, Athanassiou A, Zych A (2023) Biobased boronic ester vitrimer resin from epoxidized linseed oil for recyclable carbon fiber composites. Resour Conserv Recycl. https://doi.org/10.1016/j.resconrec.2023.107205
9. Gaglieri C, Alarcon RT, de Moura A, Bannach G (2022) Vegetable oils as monomeric and polymeric materials: a graphical review. Curr Res Green Sustain Chem. https://doi.org/10.1016/j.crgsc.2022.100343
10. Dos Santos GI, Gaglieri C, Alarcon RT, Magri R, Hartlieb M, Bannach G (2024) Passion fruit seed oil: a sustainable feedstock for additive manufacturing of renewable polymers. J Polym Environ. https://doi.org/10.1007/s10924-024-03282-w
11. Jašek V, Figalla S (2025) Vegetable oils for material applications – available biobased compounds seeking their utilities. ACS Polym Au. https://doi.org/10.1021/acspolymersau.5c00001
12. Sun Y, Sheng D, Wu H, Tian X, Xie H, Shi B, Liu X, Yang Y (2021) Bio-based vitrimer-like polyurethane based on dynamic imine bond with high-strength, reprocessability, rapid-degradability and antibacterial ability. Polymer. https://doi.org/10.1016/j.polymer.2021.124208
13. Wu J, Yu W, Zhang H, Guo J, Hu J, Li MH (2020) Fully biobased vitrimers from glycyrrhizic acid and soybean oil for self-healing, shape memory, weldable, and recyclable materials. ACS Sustain Chem Eng. https://doi.org/10.1021/acssuschemeng.0c01047
14. Zhang W, Wu J, Gao L, Zhang B, Jiang J, Hu J (2021) Recyclable, reprocessable, self-adhered and repairable carbon fiber reinforced polymers using full biobased matrices from camphoric acid and epoxidized soybean oil. Green Chem. https://doi.org/10.1039/D1GC00648G
15. Messina M, Shearer G, Petersen K (2021) Soybean oil lowers circulating cholesterol levels and coronary heart disease risk, and has no effect on markers of inflammation and oxidation. Nutrition. https://doi.org/10.1016/j.nut.2021.111343
16. Ma Y, Hu Y, Kou Z, Zhang M, Hu L, Li S, Huang Q, Jia P, Zhou Y, Chu F (2024) Soybean oil-based random copolymers based on hydrogen bond crosslinked networks as reprocessable, recyclable and multifunctional adhesive materials. Ind Crop. https://doi.org/10.1016/j.indcrop.2024.118048
17. Chaudhary ML, Patel YN, Chaudhari S, Patel R, Gupta RK (2025) Enhancing the mechanical strength of soy-based polyurethane adhesives through incorporation of schiff base diols. IJAA. https://doi.org/10.1016/j.ijadhadh.2025.104118
18. Patel R, Kumar A, Chaudhary ML, Gupta RK (2025) Design and characterization of silane-modified bio-based non-isocyanate polyurethane coatings for advanced surface applications. Materials. https://doi.org/10.3390/ma18245551
19. Liu T, Liu Z, Gu W, Zhang J, Gong S, Li J (2025) Ultratough nacre-inspired soybean protein isolate/graphene nanocomposite with flame-retardant, thermal conductivity and recyclable. Composites. https://doi.org/10.1016/j.compositesb.2024.111998
20. Fei M, Liu T, Zhao B, Otero A, Chang YC, Zhang J (2021) From glassy plastic to ductile elastomer: vegetable oil-based UV-curable vitrimers and their potential use in 3D printing. ACS Appl Polym Mater. https://doi.org/10.1021/acsapm.1c00063
21. Kamarulzaman S, Png ZM, Lim EQ, Lim IZS, Li Z, Goh SS (2023) Covalent adaptable networks from renewable resources: crosslinked polymers for a sustainable future. Chem. https://doi.org/10.1016/j.chempr.2023.04.024
22. Di Mauro C, Malburet S, Genua A, Graillot A, Mija A (2020) A Sustainable series of new epoxidized vegetable oil-based thermosets with chemical recycling properties. Biomacromolecules. https://doi.org/10.1021/acs.biomac.0c01059
23. Zhao XL, Tian PX, Li YD, Zeng JB (2022) Biobased covalent adaptable networks: towards better sustainability of thermosets. Green Chem. https://doi.org/10.1039/D2GC01325H
24. Baghban SA, Ebrahimi M, Khorasani M (2022) A facile method to synthesis of a highly acrylated epoxidized soybean oil with low viscosity: combined experimental and computational approach. Polym Test. https://doi.org/10.1016/j.polymertesting.2022.107727
25. Habib F, Bajpai M (2011) Synthesis and characterization of acrylated epoxidized soybean oil for UV-cured coatings. Chem Chem Technol. https://doi.org/10.23939/chcht05.03.317
26. Pagliaro MV, Miller HA, Bellini M, Di Vico B, Oberhauser W, Zangari G, Innocenti M, Vizza F (2021) Electrochemical reactor for sustainable transformation of bio-mass derived allyl alcohol into acrylate and pure hydrogen. Inorganica Chim Acta. https://doi.org/10.1016/j.ica.2021.120488
27. Kousaalya AB, Ayalew B, Pilla S (2019) Photopolymerization of acrylated epoxidized soybean oil: a photocalorimetry-based kinetic study. ACS Omega. https://doi.org/10.1021/acsomega.9b02680
28. Albertini E, Dalle Vacche S, Vitale A (2026) Bio-based vitrimers: chemistry, performance and applications. RSC Appl Polym. https://doi.org/10.1039/D5LP00408J
29. Bulutcu D, Eschig S (2026) Bio-based vitrimers and covalent adaptable networks – a short review. Next Sustain. https://doi.org/10.1016/j.nxsust.2025.100235
30. Zych A, Tellers J, Bertolacci L, Ceseracciu L, Marini L, Mancini G, Athanassiou A (2021) Biobased, biodegradable, self-healing boronic ester vitrimers from epoxidized soybean oil acrylate. ACS Appl Polym Mater. https://doi.org/10.1021/acsapm.0c01335
31. Cvek M, Sevcik J, Vilcakova J, Athanassiou A, Zych A (2023) Self-healing recyclable bio-based magnetic composites with boronic ester vitrimer matrix. Appl Mater Today. https://doi.org/10.1016/j.apmt.2023.101997
32. Pan X, Li J, Liu F, Hu C, Zeng Y (2023) Self-healable, weldable, and reprocessable castor oil-based poly(thiourethane-urethane) networks. J Appl Polym Sci. https://doi.org/10.1002/app.54539
33. Roig A, Agizza M, Serra À, De la Flor S (2023) Disulfide vitrimeric materials based on cystamine and diepoxy eugenol as

bio-based monomers. Eur Polym J. https://doi.org/10.1016/j.eurpolymj.2023.112185
34. Guggari S, Magliozzi F, Malburet S, Graillot A, Destarac M, Guerre M (2023) Vanillin-based epoxy vitrimers: looking at the cystamine hardener from a different perspective. ACS Sustain Chem Eng. https://doi.org/10.1021/acssuschemeng.3c00379
35. Bartoccini F, Retini M, Crinelli R, Menotta M, Fraternale A, Piersanti G (2022) Dithiol based on l-cysteine and cysteamine as a disulfide-reducing agent. J Org Chem. https://doi.org/10.1021/acs.joc.2c01050
36. Paramarta A, Webster DC (2017) The exploration of Michael-addition reaction chemistry to create high performance, ambient cure thermoset coatings based on soybean oil. Prog Org Coat. https://doi.org/10.1016/j.porgcoat.2017.04.004
37. Taplan C, Guerre M, Du Prez FE (2021) Covalent adaptable networks using β-amino esters as thermally reversible building blocks. J Am Chem Soc. https://doi.org/10.1021/jacs.1c03316
38. Peyrton J, Avérous L (2021) Aza-Michael reaction as a greener, safer, and more sustainable approach to biobased polyurethane thermosets. ACS Sustain Chem Eng. https://doi.org/10.1021/acssuschemeng.1c00312
39. Bláha M, Trhlíková O, Podešva J, Abbrent S, Steinhart M, Dybal J, Dušková-Smrčková M (2018) Solvent-free, catalyst-free aza-Michael addition of cyclohexylamine to diethyl maleate: reaction mechanism and kinetics. Tetrahedron. https://doi.org/10.1016/j.tet.2017.11.033
40. Lorenz N, Dyer WE, Kumru B (2025) Exploring the cure state dependence of relaxation and the vitrimer transition phenomena of a disulfide-based epoxy vitrimer. J Polym Sci. https://doi.org/10.1002/pol.20250463
41. Gupta J, Rajamani P (2023) Size- and surface functionalization-driven molecular interaction of CdSe quantum dots with jack bean urease: multispectroscopic, thermodynamic, and AFM approach. Environ Sci Pollut Res. https://doi.org/10.1007/s11356-023-25356-3
42. Colucci G, Sacchi F, Bondioli F, Messori M (2925) 3D printing of lignin-based polymeric composites obtained using liquid crystal display as a vat photopolymerization technique. Polym Int. https://doi.org/10.1002/pi.6783
43. Li X, Wang D, Zhao L, Hou X, Liu L, Feng B, Li M, Zheng P, Zhao X, Wei S (2021) UV LED curable epoxy soybean-oil-based waterborne PUA resin for wood coatings. Prog Org Coat. https://doi.org/10.1016/j.porgcoat.2020.105942
44. Roudsari GM, Mohanty AK, Misra M (2014) Study of the curing kinetics of epoxy resins with biobased hardener and epoxidized soybean oil. ACS Sustain Chem Eng. https://doi.org/10.1021/sc500176z
45. Desmet GB, D'Hooge DR, Omurtag PS, Espeel P, Marin GB, Du Prez FE, Reyniers MF (2016) Quantitative first-principles kinetic modeling of the aza-Michael addition to acrylates in polar aprotic solvents. J Org Chem. https://doi.org/10.1021/acs.joc.6b02218
46. Bosica G, Debono AJ (2014) Uncatalyzed, green aza-Michael addition of amines to dimethyl maleate. Tetrahedron. https://doi.org/10.1016/j.tet.2014.06.124
47. Abe I, Shibata M (2024) Bio-based self-healing epoxy vitrimers with dynamic imine and disulfide bonds derived from vanillin, cystamine, and dimer diamine. Molecules. https://doi.org/10.3390/molecules29204839
48. Kasetaite S, De la Flor S, Serra A, Ostrauskaite J (2018) Effect of selected thiols on cross-linking of acrylated epoxidized soybean oil and properties of resulting polymers. Polymers. https://doi.org/10.3390/polym10040439
49. Coste G, Negrell C, Averous L, Caillol S (2022) Green synthesis of biobased soft foams by the aza-Michael reaction. ACS Sustain Chem Eng. https://doi.org/10.1021/acssuschemeng.2c01885
50. Auclair N, Kaboorani A, Riedl B, Landry V (2020) Effects of surface modification of cellulose nanocrystals (CNCs) on curing behavior, optical, and thermal properties of soybean oil bio-nanocomposite. J Coat Technol Res. https://doi.org/10.1007/s11998-019-00237-y
51. Golovnev NN, Kirik SD, Gerasimov VS, Belash MY (2013) Synthesis and properties of cystaminium salts with d-metal acid and tetrahalide anions. Russ J Inorg Chem. https://doi.org/10.1134/S0036023613050082
52. Leshok DY, Golovnev NN, Kirik SD (2015) Cystamindi-ium tetrachlorocuprate [NH3(CH2)2SS(CH2)2NH3][CuCl4]: synthesis, crystal structure, and thermal decomposition. Powder Diffr. https://doi.org/10.1017/S0885715614001390
53. Khalafi HR, Ehsani M, Khonakdar HA (2021) Investigation of the cure kinetics and thermal stability of an epoxy system containing cystamine as curing agent. Polym Adv Technol. https://doi.org/10.1002/pat.5174
54. Behera D, Banthia AK (2008) Synthesis, characterization, and kinetics study of thermal decomposition of epoxidized soybean oil acrylate. J Appl Polym Sci. https://doi.org/10.1002/app.28350
55. Gooranorimi A, Mousavifard SM, Mohseni M, Yahyaei H, Makki H (2025) Effective cross-link density as a metric for structure–property relationships in complex polymer networks: insights from acrylic melamine systems. ACS Appl Polym Mater. https://doi.org/10.1021/acsapm.5c01155
56. Cosola A, Conti R, Grützmacher H, Sangermano M, Roppolo I, Pirri CF, Chiappone A (2020) Multiacrylated cyclodextrin: a bio-derived photocurable macromer for vat 3D printing. Macromol Mater Eng. https://doi.org/10.1002/mame.202000350
57. Simon GP, Allen PEM, Williams DRG (1991) Properties of dimethacrylate copolymers of varying crosslink density. Polymer. https://doi.org/10.1016/0032-3861(91)90337-I
58. Hammer L, Van Zee NJ, Nicolaÿ R (2021) Dually crosslinked polymer networks incorporating dynamic covalent bonds. Polymers. https://doi.org/10.3390/polym13030396
59. Berne D, Laviéville S, Leclerc E, Caillol S, Ladmiral V, Bakkali-Hassani C (2025) How to characterize covalent adaptable networks: a user guide. ACS Polym Au. https://doi.org/10.1021/acspolymersau.5c00004
60. Ricarte RG, Shanbhag S (2024) A tutorial review of linear rheology for polymer chemists: basics and best practices for covalent adaptable networks. Polym Chem. https://doi.org/10.1039/d3py01367g
61. Soavi G, Portone F, Battegazzore D, Paravidino C, Arrigo R, Pedrini A, Pinalli R, Fina A, Dalcanale E (2023) Phenoxy resin-based vinylogous urethane covalent adaptable networks. React Funct Polym. https://doi.org/10.1016/j.reactfunctpolym.2023.105681
62. Tellers J, Pinalli R, Soliman M, Vachon J, Dalcanale E (2019) Reprocessable vinylogous urethane cross-linked polyethylene: via reactive extrusion. Polym Chem. https://doi.org/10.1039/c9py01194c
63. Guo Z, Jiao X, Wei K, Wu J, Hu J (2023) Comprehensive itaconic acid-based vitrimers via one-pot inverse vulcanization. Green Chem. https://doi.org/10.1039/D3GC00899A
64. Zhang B, Yuan C, Zhang W, Dunn ML, Qi HJ, Liu Z, Yu K, Ge Q (2019) Recycling of vitrimer blends with tunable thermomechanical properties. RSC Adv. https://doi.org/10.1039/C9RA00015A
65. Wu NH, Liu YL (2025) Biomass-based diketoenamine vitrimers: synthesis, properties, reprocessing, and closed-loop chemical recycling. ACS Appl Polym Mater. https://doi.org/10.1021/acsapm.4c03127
66. Chien SY, Wang J, Liu YL (2024) Biodegradable polyester-based vitrimers exhibiting transesterification-induced topography isomerization under recycling. ACS Appl Polym. https://doi.org/10.1021/acsapm.4c01539

67. Sibilia D, Amendolea M, Sangiovanni R, Bragaglia M, Nicoletti F, Filetici P, D'Addona A, Nanni F, Dassatti L, Nocca G (2024) Biodegradation study of biomaterials composed of acrylated epoxidized soybean oil: an in vitro study. Biomed Res Int. https://doi.org/10.1155/bmri/7100988
68. Hu C, Lu E, Lacour L, Delsuc N, Bresson B, Mallet JM, Fattacciioli J (2024) Shaping, degradation and drug release of biosourced particles made from acrylated vegetable oils. https://doi.org/10.26434/chemrxiv-2024-3c42z
69. Damonte G, Vallin A, Giribaldi L, Pellis A, Hakkarainen M, Subramaniyan S, Campaner P, Monticelli O (2025) A sustainable approach to recycling of polylactic acid with environmentally friendly reagents. Sustain Mater Technol. https://doi.org/10.1016/j.susmat.2025.e01320
70. Damonte G, Dullaert L, Pellis A, Giribaldi L, Monticelli O (2026) On the upcycling of PCL to produce building blocks for the development of PCL-PLA copolymers. Eur Polym J. https://doi.org/10.1016/j.eurpolymj.2026.114563

Publisher's Note Springer Nature remains neutral with regard to jurisdictional claims in published maps and institutional affiliations.